

# Error tolerance of topological codes with independent bit-flip and measurement errors

Ruben S. Andrist,<sup>1</sup> Helmut G. Katzgraber,<sup>2,1</sup> H. Bombin,<sup>3</sup> and M. A. Martin-Delgado<sup>4</sup>

<sup>1</sup>*Santa Fe Institute, 1399 Hyde Park Road, Santa Fe, New Mexico 87501, USA*

<sup>2</sup>*Department of Physics and Astronomy, Texas A&M University, College Station, Texas 77843-4242, USA*

<sup>3</sup>*Yukawa Institute for Theoretical Physics, Kyoto University, Sakyo, Kyoto 606-8502, Japan*

<sup>4</sup>*Departamento de Física Teórica I, Universidad Complutense, 28040 Madrid, Spain*

Topological quantum error correction codes are currently among the most promising candidates for efficiently dealing with the decoherence effects inherently present in quantum devices. Numerically, their theoretical error threshold can be calculated by mapping the underlying quantum problem to a related classical statistical-mechanical spin system with quenched disorder. Here, we present results for the general fault-tolerant regime, where we consider both qubit and measurement errors. However, unlike in previous studies, here we vary the strength of the different error sources independently. Our results highlight peculiar differences between toric and color codes. This study complements previous results published in *New J. Phys.* **13**, 083006 (2011).

PACS numbers: 03.67.Pp, 75.40.Mg, 11.15.Ha, 03.67.Lx

The quest for building a reliable quantum computer involves multiple fields of research, such as several branches of computer science, theoretical and experimental physics, mathematics, and engineering [1, 2]. Most notably, disordered spin systems and lattice gauge theories [3–6] in statistical physics have played a pivotal role in the understanding of the theoretical error tolerance of topological quantum computing models in quantum information theory [3, 7–11]. The main driver for this fruitful synergy across disciplines was the discovery that methods from statistical physics allow for the numerical study of quantum error correction codes [12–18]. More specifically, error fluctuations in topologically protected codes map [3] directly onto classical spin models with tunable disorder. The level of noise in the quantum code then corresponds to the amount of quenched disorder in a classical spin system. In practice, this means that by carefully analyzing the critical behavior of the classical system, we can learn how resilient a topological code is to a particular source of errors.

The very same approach can also be used to investigate fault-tolerant error correction [19–21], which takes the possibility of faulty measurements during the error-correction procedure into account. This is particularly exciting because topological codes [22] allow for fault-tolerant quantum computation without resorting to code concatenation [3, 23–26]. Instead, the new resource is the nontrivial topology of the lattice on which the physical qubits are arranged. The topological quantum code, in turn, is defined by the pattern of the arrangement and the way in which check operators act on these qubits. The key property of these check operators (also known as stabilizers), is that their support is local on the qubits forming the lattice. This locality property is absent in concatenated codes and is beneficial for experimental realizations. Moreover, as long as the external errors act also locally on the code, it is possible to protect the encoded quantum information because the encoded logical qubits are entangled states that spread out globally across the whole system. While implementing such sys-

tems might seem to be an insurmountable effort at this time, recently, a complete error-correction code for arbitrary errors using a minimal topological color code has been realized experimentally in a trapped-ion platform [27] that paves the way towards the experimental realization of topological codes, such as the Kitaev code or the color codes in two-dimensional setups [28–32]. As such, gaining a deeper understanding of the interplay between different error sources is of current importance.

Remarkably, assuming that both bit-flip errors and measurement errors occur at the same average rate, previous numerical results [6] suggest that topological color codes [23] exhibit an improved error tolerance over the toric code [22]. While this is potentially only true in the ideal scenario where all physical operations are noise free, it does serve as a guide when comparing the performance of both models on an equal footing. Here, we further investigate this observation by extending the numerical results to qubit and measurement errors of different average strength.

The paper is organized as follows. Section I provides a brief introduction to the toric code and topological color codes in the fault-tolerant regime. Section II summarizes the mappings to classical lattice gauge theories as derived in Ref. [6] for color codes and Ref. [4] for the toric code. In Sec. III we explain the numerical tools used for our extended analysis, followed by the results in Sec. IV, as well as concluding remarks.

## I. TOPOLOGICAL STABILIZER CODES

A stabilizer code  $\mathcal{C}$  of length  $n$  is a subspace of the Hilbert space of a set of  $n$  physical qubits [16]. The code is defined by means of the stabilizer group  $\mathcal{S} \subset \mathcal{P}_n$  of Pauli operators, which are tensor products of Pauli matrices of length  $n$ :

$$\mathcal{P}_n := \langle 1, X_1, Z_1, \dots, X_n, Z_n \rangle. \quad (1)$$

The stabilizer group leaves invariant the quantum states belonging to the code:

$$|\psi\rangle \in \mathcal{C} \iff \forall O \in \mathcal{S} \quad O|\psi\rangle = |\psi\rangle. \quad (2)$$

The Pauli operator  $-1$  is excluded from  $\mathcal{S}$ . To fully characterize the code it is sufficient to define the generators of  $\mathcal{S}$ :

$$\mathcal{G} := \langle 1, g_1, \dots, g_k \rangle. \quad (3)$$

The normalizer  $\mathcal{N}(\mathcal{S})$  of  $\mathcal{S}$  plays a fundamental role in error correction. It is defined by the operators  $O$  satisfying:

$$O \in \mathcal{N}(\mathcal{S}) \iff OS = SO, \quad (4)$$

which implies that the code space  $\mathcal{C}$  is left invariant by  $\mathcal{N}(\mathcal{S})$ . When the operators of the normalizer do not belong to the stabilizer itself, then they act in a non-trivial way on the encoded states.

Active error correction is necessary to protect the error-prone logical state: we need to measure a set of generators of  $\mathcal{S}$ . The result of these measurements is called the syndrome—the signature of which error has occurred. Errors can be corrected as long as the syndromes allow us to discriminate among possible errors. As correctable errors always form a vector space, it is enough to consider Pauli operators, which form a basis. A Pauli error  $e$  is said to be undetectable if it belongs to the set  $\mathcal{N}(\mathcal{S}) - \mathcal{S}$ . In this case, the syndrome provides no information:

$$\forall s \in \mathcal{S} \quad s e |\psi\rangle = e s' |\psi\rangle = |\psi\rangle. \quad (5)$$

A set of Pauli errors  $E$  is said to be correctable if, and only if,

$$E^\dagger E \cap \mathcal{N}(\mathcal{S}) \in \mathcal{S}. \quad (6)$$

Topological stabilizer codes are peculiar instances of stabilizer codes employing a regular arrangement of qubits on a topologically non-trivial surface [33] and local stabilizer operators. Because both codes are Calderbank-Shor-Steane codes [14, 15], bit-flip and phase errors can be corrected independently and analogously. Here we focus only on bit-flip errors occurring at a rate  $p$ .

*Toric code.* The physical qubits are arranged on the edges of a two-dimensional lattice, with stabilizers at each vertex being the tensor product of  $\hat{Z}$  operators for adjacent qubits [22]. Thus flipping qubit  $Q_\ell$  changes the sign of the measured eigenvalue for the check operators at either end of the edge  $\ell$ . The first example of such a topological code was the Kitaev toric code defined with a square-lattice arrangement. In this case, each stabilizer operator  $\hat{Z}^{\otimes 4}$  is the tensor product of exactly four  $\hat{Z}$  operators.

*Topological color codes.* Initially conceived to expand the computational capabilities of topological codes by increasing the set of topological gates that can be applied [23, 24], here we consider a hexagonal arrangement of the physical qubits, with stabilizers  $\hat{Z}^{\otimes 6}$  on each plaquette acting on the adjacent qubits.

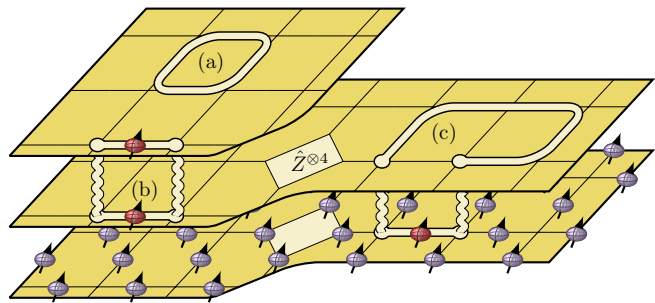


Figure 1: (Color online) Stacked layers representing the mapped model for the fault-tolerant toric code. Qubits reside on the edges and stabilizer operators  $\hat{Z}^{\otimes 4}$  act on the qubits surrounding each vertex. (a) Horizontal loops correspond to the usual local equivalence of the toric code: flipping the four qubits around a plaquette leaves the error syndrome invariant. (b) The second type of local equivalence involves measurement errors which are represented by vertical links connecting stabilizer operators. (c) The resulting model consists of spatial and time-like links forming a three-dimensional cubic lattice.

*Error correction.* For all check operators, encoded states satisfy  $\hat{Z}|\psi\rangle = |\psi\rangle$ . Such states exist because the group generated by check operators, called the stabilizer group, does not contain  $-1$ , so that in particular check operators commute with each other. The dimension of the encoded subspace depends only on the topology of the surface where the code lives. For example, a regular lattice with periodic boundary conditions has the topology of a torus and encodes two logical qubits [23].

*Fault-tolerant regime.* With measurements being faulty at a rate  $q$ , new errors are introduced involuntarily during the error-correction procedure. To detect local inconsistencies with the code, check operators need to be measured repeatedly over time and error correction amounts to guessing the correct error history  $E$  among those that are compatible with the recorded measurement outcomes. Such an error history is typically comprised of some combination of bit-flip and measurement errors. Indeed, many error histories have an equivalent effect, and thus the ideal strategy is to compute which equivalence class  $\bar{E}$  happened with the highest probability  $P(\bar{E})$ . Therefore, error correction is highly successful when for typical errors there is a class that dominates over the others.

## II. MAPPING TO LATTICE GAUGE THEORIES

For both types of topological stabilizer codes introduced in the previous section, the mapping of the setup to a classical spin system produces a lattice gauge theory with disorder [3, 6]. For a side-by-side comparison, it is instructive to describe both in terms of their local equivalences. The results of the respective mappings (with

some minor adjustments to match the notations) can be summarized as follows.

*Toric codes ( $\mathbb{Z}_2$  lattice gauge theory).* The toric code for bit-flip errors occurs on the edges of a square lattice with stabilizer operators at each vertex acting on the four adjacent qubits (see Fig. 1). Fault tolerance is added by stacking multiple of these lattices and connecting the vertices vertically to a three-dimensional cubic grid. We can then interpret the vertical axis as time with each vertical edge representing a measurement of the stabilizer operator it connects.

In addition to the regular local equivalence of flipping four qubits around a horizontal plaquette, this stacked model also has a second type that consists of flipping the same qubit in adjacent layers along with the two measurements connecting them. This equivalence is a vertical plaquette in the three-dimensional lattice and represents the scenario of two consecutive bit-flip errors which go unnoticed because of two concurrent measurement errors.

The probability of an error arbitrary history  $E$ , consisting of  $h$  bit-flip errors and  $v$  faulty measurements, can be written as

$$\begin{aligned} \mathcal{P}(E) &= (1-p)^{H-h} p^h (1-q)^{V-v} q^v \\ &\propto \left(\frac{p}{1-p}\right)^h \left(\frac{q}{1-q}\right)^v, \end{aligned} \quad (7)$$

where  $p$  is the bit-flip rate and  $q$  the measurement error rate, while both  $H$  (total number of qubits) and  $V$  (total number of measurements) are constants of the cubic lattice.

A specific error history  $E$  can be represented by a set of variables  $\tau_\ell \in \{\pm 1\}$ , each indicating whether the qubit or measurement corresponding to edge  $\ell$  is faulty. Furthermore, we can enumerate all histories in the error class of

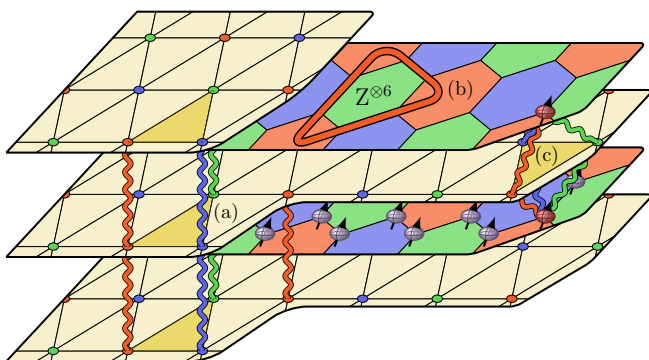


Figure 2: (Color online) Resulting lattice gauge theory for topological color codes on a hexagonal lattice. (a) The horizontal layers are alternating triangular and hexagonal lattices, with time corresponding to the vertical axis. Qubits reside on the vertices of the trivalent (hexagonal) lattice. (b) Colored loops in the hexagonal planes correspond to bit-flip error chains. (c) Vertical loops involve measurement errors between two time slices. This scenario is analogous to the case of two unnoticed consecutive errors for the toric code.

$E$  (i.e., those that differ only by local equivalences) by attaching a binary variable  $\sigma_{h,v} \in \pm 1$  to each equivalence. To numerically sample from these, one then constructs a classical Hamiltonian which has Boltzmann weights proportional to Eq. (7):

$$\mathcal{H}_E = -J \sum_{j \in \ell_Q} \tau_j \sigma_h^{\otimes 2} \sigma_v^{\otimes 2} - K \sum_{k \in \ell_M} \tau_k \sigma_v^{\otimes 4}, \quad (8)$$

Note that the first sum (which iterates over all qubits  $Q$ , i.e., horizontal links) essentially counts the number of flipped qubits. By definition, a qubit is flipped if the product of  $\tau_j$  and all the equivalences it is affected by (two horizontal and two vertical ones) is negative. Similarly, the second sum iterates over all measurements  $M$  and adds up the number of faulty ones. Therefore, we can see that the correct Boltzmann weights are produced with

$$e^{-2\beta J} = p/(1-p), \quad e^{-2\beta K} = q/(1-q), \quad (9)$$

which is called the Nishimori condition [34]. The Hamiltonian in Eq. (8) is equivalent to the one given by Dennis *et al.* [3], however, with separated terms for qubit and measurement errors.

*Color codes (tricolored lattice gauge theory).* For topological color codes, consider a three-dimensional lattice consisting of stacked triangular and hexagonal layers, with qubits residing on intermediate hexagonal layers. There is a stabilizer operator  $\hat{Z}^{\otimes 6}$  for each of the hexagonal tiles, acting on the six qubits surrounding the plaquette.

As for the toric code, there are again two distinct types of elementary equivalences. The first is a horizontal loop consisting of the six qubits around a plaquette, while the second consists of adjacent qubits in two layers, connected by three measurement errors (see Fig. 2). This represents again the scenario of two subsequent qubit flips on the same qubit, which remain unnoticed because of three concurrent measurement errors. The resulting Hamiltonian takes the form

$$\mathcal{H}_E = -J \sum_{j \in Q} \tau_j \sigma_h^{\otimes 3} \sigma_v^{\otimes 2} - K \sum_{k \in M} \tau_k \sigma_v^{\otimes 6}, \quad (10)$$

with identical requirements for the constants  $J$  and  $K$ . This corresponds to the Hamiltonian calculated by Andrist *et al.* (See Refs. [6, 35] for details).

### III. NUMERICAL METHODS

Based on the Hamiltonians in Eq. (8) for the toric code and Eq. (10) for color codes, the error threshold for a particular code is given by the largest error rates for which the model remains in an ordered state at the temperature  $T$  specified by the Nishimori condition. Dennis *et al.* [3] have demonstrated that this property is found at the multicritical point of the  $p$ - $T$  ( $p$  the bit-flip error rate) phase

Table I: Simulation parameters:  $L$  is the layer size,  $M$  is the number of layers,  $N_{\text{sa}}$  is the number of disorder samples,  $t_{\text{eq}} = 2^b$  is the number of equilibration sweeps,  $T_{\text{min}}$  ( $T_{\text{max}}$ ) is the lowest (highest) temperature, and  $N_{\text{T}}$  is the number of temperatures used for a given error rate  $p$ . The corresponding values of  $q$  are given by the simulation paths chosen, namely  $q = 2p$ ,  $q = p$ , and  $q = p/2$ .

$p$	$L$	$M$	$N_{\text{sa}}$	$b$	$T_{\text{min}}$	$T_{\text{max}}$	$N_{\text{T}}$
0.00	6, 9	6, 8	1600	15	1.20	2.00	64
0.00	12	12	800	15	1.20	2.00	64
0.02	6, 9	6, 8	1600	16	0.90	1.80	52
0.02	12	12	800	17	0.90	1.80	52
0.03–0.039	6, 9	6, 8	1600	17	0.70	1.40	52
0.03–0.039	12	12	800	19	0.70	1.40	52
0.04–0.060	6, 9	6, 8	1600	18	0.50	1.20	52
0.04–0.060	12	12	800	20	0.50	1.20	52

diagram where the Nishimori line intersects the phase boundary. For independent qubit and measurement error rates, the Nishimori condition translates to a *Nishimori sheet* in the three-dimensional parameter space spanned by  $p$ ,  $q$  and the model’s temperature  $T = 1/\beta$ . Note that the purpose of this “virtual” temperature is merely to achieve the desired Boltzmann statistics via Eq. (9), while any physical temperature effects in the quantum device are implicitly captured by the error rates  $p$  and  $q$ .

We use large-scale Monte Carlo simulations to analyze the phase diagram along different projections, namely  $p = 2q$  and  $p = q/2$ . In both cases we expect to find the system in an ordered Higgs phase for weak disorder and low temperatures  $T$ . This indicates that error histories observed at these error rates typically exhibit only small fluctuations. Once the phase boundary is crossed, the system enters the disordered confinement phase, indicating that the topologically encoded information is vulnerable to failures.

The crossing point is determined as follows. For increasingly larger error rates  $p$  and  $q$ , we use the peak position in the measured system’s susceptibility as done in Ref. [4], as well as the skewness of the Wilson loop distribution [6] to locate the phase transition temperature  $T_c(p, q)$ . As long as this transition occurs at a higher temperature than the one specified by the Nishimori condition, we know that the system still exhibits an ordered state. Because the error rates  $p$  and  $q$  are merely parameters to generate the quenched random interactions, these calculations need to be repeated for many independent disorder realizations to obtain the desired statistical-mechanical average. This and the fact that disordered lattice gauge theories are inherently hard to simulate necessitates considerable numerical efforts for every single point generated in the phase diagram in Fig. 3. To mitigate this challenge, we use the parallel tempering Monte Carlo technique [36], with the detailed simulation parameters listed in Table I. Equilibration for

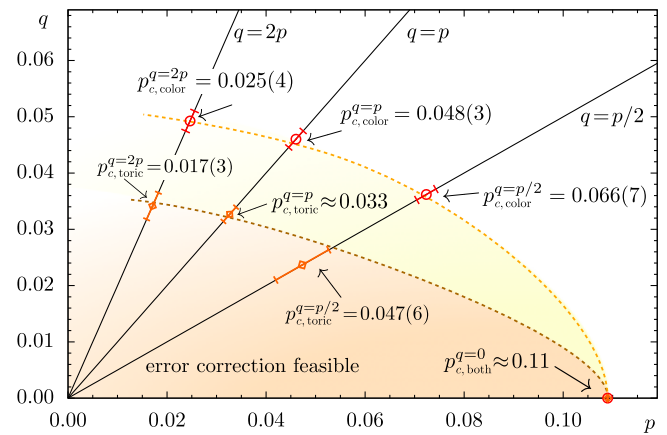


Figure 3: (Color online) Summary of the numerically calculated error thresholds in context of the previous results. The plot indicates the phase boundaries of the ordered phase for both types of codes, projected onto the Nishimori surface where the mapping to the quantum setup is valid. The estimates indicate that the difference in resilience remains even for non-matching error rates. Simulations for  $p \rightarrow 0$  are difficult and we have no estimates for this regime.

each sample is tested by a logarithmic binning of the data. Once the last three bins agree within statistical error bars, the system is deemed to be in thermal equilibrium.

#### IV. RESULTS

Our results are summarized in Fig. 3, which also includes estimates of critical points computed in previous publications [3, 4, 6, 7]. In principle, the parametric space of the models constructed in Sec. II is three dimensional, spanned by  $p$ ,  $q$  and  $T$ . However, since the Nishimori surface represents the locus of points where the mapping from the quantum setup is valid, we can render the results in a  $p$ - $q$  plot by projecting onto the Nishimori sheet along the temperature axis. The colored areas then represent the portion of phase space for which the Nishimori sheet is within the ordered phase of the model.

When measurement errors are not taken into account, it was shown in Refs. [3, 7] that both codes have equal thresholds of  $p_c \approx 0.109$ . This is indicated in Fig. 3 by both phases intercepting the horizontal axis at the same point. Ohno *et al.* [4] have estimated the threshold for the toric code at equal error rates to be  $p_c^{q=p} \approx 0.03$ . Remarkably, the error resilience of topological color codes under the same circumstances was found [6] to be substantially higher at  $p_c^{q=p} \approx 0.048(3)$ . To further the understanding of this curious difference, we complement these previous results with estimates for non-matching error rates at  $q = 2p$  and  $q = p/2$ . In both cases, there is still a notable difference between the two types of codes. It thus seems that color codes are more resilient to noise

and measurement errors than toric codes across the whole Nishimori sheet. The lines in Fig. 3 are meant as guides to the eye. Simulating more points in the phase diagram is extremely difficult. However, we feel that the results are robust within error bars.

## V. CONCLUSIONS

Our numerical results indicate that the difference in error resilience between the toric code and topological color codes persists when bit-flip and measurement errors occur at different rates. Only in the limit of a vanishing measurement error rate the two lines in Fig. 3 converge to a common point, i.e., both toric and color codes have the same error threshold to bit-flip errors. Exploring the regime where measurement errors are far more common than bit-flip errors is extremely difficult numerically because of the anisotropy of the resulting lattice gauge theory. However, for a large portion of the phase diagram in the  $p$ - $q$  plane both topological schemes show different error tolerance. Gaining a complete understanding of the underlying cause for the differences between the two types of topological error-correction codes in the fault-tolerant regime will require new analysis approaches by improving the error model with more realistic features like taking into account the unavoidable noise introduced by real physical operations during the correction protocol. Whether the differences between both codes vanish under external noise remains an open problem, and this may also require more detailed studies of lattice gauge theories with quenched bond disorder. This, however,

is a numerically and analytically extremely challenging problem.

## Acknowledgments

The authors thank ETH Zurich for CPU time on the Brutus cluster, the Santa Fe Institute for CPU time on the Scoville cluster, and the Centro de Supercomputacion y Visualizacion de Madrid (CeSViMa) for access to the Magerit cluster. M.A.M.-D. and H.B. acknowledge financial support from the Spanish MINECO Grant No. FIS2012-33152, the Spanish MINECO Grant No. FIS2015-67411, and the CAM research consortium QUITEMAD+, Grant No. S2013/ICE-2801. The research of M.A.M.-D. has been supported in part by the U.S. Army Research Office through Grant No. W911N F-14-1-0103. H.G.K. acknowledges support from the National Science Foundation (Grant No. DMR-1151387) and the Swiss National Science Foundation (Grant No. PP002-114713). Part of the research of H.G.K. is based upon work supported in part by the Office of the Director of National Intelligence (ODNI), Intelligence Advanced Research Projects Activity (IARPA), via MIT Lincoln Laboratory Air Force Contract No. FA8721-05-C-0002. The views and conclusions contained herein are those of the authors and should not be interpreted as necessarily representing the official policies or endorsements, either expressed or implied, of ODNI, IARPA, or the U.S. Government. The U.S. Government is authorized to reproduce and distribute reprints for governmental purpose notwithstanding any copyright annotation thereon.

- 
- [1] M. A. Nielsen and I. L. Chuang, *Quantum Computation and Quantum Information* (Cambridge University Press, Cambridge, 2000).
  - [2] A. Galindo and M. A. Martin-Delgado, *Information and Computation: Classical and Quantum Aspects*, Rev. Mod. Phys. **74**, 347 (2002).
  - [3] E. Dennis, A. Kitaev, A. Landahl, and J. Preskill, *Topological quantum memory*, J. Math. Phys. **43**, 4452 (2002).
  - [4] T. Ohno, G. Arakawa, I. Ichinose, and T. Matsui, *Phase structure of the random-plaquette  $Z_2$  gauge model: accuracy threshold for a toric quantum memory*, Nucl. Phys. B **697**, 462 (2004).
  - [5] C. Wang, J. Harrington, and J. Preskill, *Confinement-Higgs transition in a disordered gauge theory and the accuracy threshold for quantum memory*, Ann. Phys. **303**, 31 (2003).
  - [6] R. S. Andrist, H. G. Katzgraber, H. Bombin, and M. A. Martin-Delgado, *Tricolored Lattice Gauge Theory with Randomness: Fault-Tolerance in Topological Color Codes*, New J. Phys. **13**, 083006 (2011).
  - [7] H. G. Katzgraber, H. Bombin, and M. A. Martin-Delgado, *Error Threshold for Color Codes and Random 3-Body Ising Models*, Phys. Rev. Lett. **103**, 090501 (2009).
  - [8] M. Ohzeki, *Accuracy thresholds of topological color codes on the hexagonal and square-octagonal lattices*, Phys. Rev. E **80**, 011141 (2009).
  - [9] R. Raussendorf and J. Harrington, *Fault-Tolerant Quantum Computation with High Threshold in Two Dimensions*, Phys. Rev. Lett. **98**, 190504 (2007).
  - [10] A. G. Fowler, D. S. Wang, and L. C. L. Hollenberg, *Surface code quantum error correction incorporating accurate error propagation*, Quant. Inf. Comput. **11**, 8 (2011).
  - [11] A. Landahl, J. T. Anderson, and P. Rice, *Fault-tolerant quantum computing with color codes*, (arXiv:quant-ph/1108.5738) (2011).
  - [12] P. W. Shor, *Scheme for reducing decoherence in quantum computer memory*, Phys. Rev. A **52**, R2493 (1995).
  - [13] A. M. Steane, *Error Correcting Codes in Quantum Theory*, Phys. Rev. Lett. **77**, 793 (1996).
  - [14] A. R. Calderbank and P. W. Shor, *Good quantum error-correcting codes exist*, Phys. Rev. A **54**, 1098 (1996).
  - [15] A. Steane, *Multiple-Particle Interference and Quantum Error Correction*, Proc. Roy. Soc. Lond. A **452**, 2551 (1996).
  - [16] D. Gottesman, *Class of quantum error-correcting codes saturating the quantum Hamming bound*, Phys. Rev. A **54**, 1862 (1996).

- [17] C. H. Bennett, D. P. Divincenzo, J. A. Smolin, and W. K. Wootters, *Mixed-state entanglement and quantum error correction*, Phys. Rev. A **54**, 3824 (1996).
- [18] B. M. Terhal, *Quantum error correction for quantum memories*, Rev. Mod. Phys. **87**, 307 (2015).
- [19] P. W. Shor, in *Proc. of the 37th Symp. on the Foundations of Computer Science* (IEEE Computer Society, 1996), p. 56.
- [20] E. Knill, R. Laflamme, and W. Zurek, *Threshold Accuracy for Quantum Computation* (1996), (arXiv:quant-ph/9610011).
- [21] D. Aharonov and M. Ben-Or, in *Proc. of the 29th annual ACM symp. on Th. of computation., El Paso TX* (ACM, 1997), p. 188.
- [22] A. Y. Kitaev, *Fault-tolerant quantum computation by anyons*, Ann. Phys. **303**, 2 (2003).
- [23] H. Bombin and M. A. Martin-Delgado, *Topological Quantum Distillation*, Phys. Rev. Lett. **97**, 180501 (2006).
- [24] H. Bombin and M. A. Martin-Delgado, *Topological Computation without Braiding*, Phys. Rev. Lett. **98**, 160502 (2007).
- [25] H. Bombin and M. A. Martin-Delgado, *Exact topological quantum order in  $D = 3$  and beyond: Branyons and brane-net condensates*, Phys. Rev. B **75**, 075103 (2007).
- [26] C. Nayak, S. H. Simon, A. Stern, M. Freedman, and S. Das Sarma, *Non-Abelian anyons and topological quantum computation*, Rev. Mod. Phys. **80**, 1083 (2008).
- [27] D. Nigg, M. Mueller, E. A. Martinez, P. Schindler, M. Hennrich, T. Monz, M. A. Martin-Delgado, and R. Blatt, *Experimental Quantum Computations on a Topologically Encoded Qubit*, Science **345**, 302 (2014).
- [28] M. Niedermayr, K. Lakhmankiy, M. Kumph, S. Partel, J. Edlinger, M. Brownmutter, and R. Blatt, *Cryogenic surface ion trap based on intrinsic silicon*, N. J. Phys. **16**, 113068 (2014).
- [29] R. Barends, J. Kelly, A. Megrant, A. Veitia, D. Sank, E. Jeffrey, T. C. White, J. Mutus, A. G. Fowler, B. Campbell, et al., *Superconducting quantum circuits at the surface code threshold for fault tolerance*, Nature **508**, 500 (2014).
- [30] A. D. Córcoles, E. Magesan, S. J. Srinivasan, A. W. Cross, M. Steffen, J. M. Gambetta, and J. M. Chow, *Demonstration of a quantum error detection code using a square lattice of four superconducting qubits*, Nature Commun. **6**, 6979 (2015).
- [31] R. Kueng, D. M. Long, A. C. Doherty, and S. T. Flammia, *Comparing Experiments to the Fault-Tolerance Threshold* (2015), (arXiv:quant-ph/1510.05653).
- [32] M. Müller, A. Rivas, E. A. Martínez, D. Nigg, P. Schindler, T. Monz, R. Blatt, and M. A. Martin-Delgado, *Iterative Phase Optimisation of Elementary Quantum Error Correcting Codes* (2016), (arXiv:quant-ph/1603.00402).
- [33] H. Bombin and M. A. Martin-Delgado, *Homological error correction: Classical and quantum codes*, J. Math. Phys. **48**, 052105 (2007).
- [34] H. Nishimori, *Internal Energy, Specific Heat and Correlation Function of the Bond-Random Ising Model*, Prog. Theor. Phys. **66**, 1169 (1981).
- [35] R. S. Andrist, H. Bombin, H. G. Katzgraber, and M. A. Martin-Delgado, *Optimal error correction in topological subsystem codes*, Phys. Rev. A **85**, 050302 (2012).
- [36] K. Hukushima and K. Nemoto, *Exchange Monte Carlo method and application to spin glass simulations*, J. Phys. Soc. Jpn. **65**, 1604 (1996).